Phys. Status Solidi B **248**, No. 11, 2672–2675 (2011) / **DOI** 10.1002/pssb.201100121

physica status solidi b
www.pss-b.com
basic solid state physics

Magnetoconductance of carbon nanotubes probed in parallel magnetic fields up to 60 T

Sung Ho Jhang[*,1], Magdalena Margańska[2], Miriam del Valle[2], Yurii Skourski[3], Milena Grifoni[2], Joachim Wosnitza[3], and Christoph Strunk[1]

[1] Institute of Experimental and Applied Physics, University of Regensburg, 93040 Regensburg, Germany
[2] Institute for Theoretical Physics, University of Regensburg, 93040 Regensburg, Germany
[3] Dresden High Magnetic Field Laboratory, Helmholtz-Zentrum Dresden-Rossendorf, 01324 Dresden, Germany

Received 30 April 2011, revised 29 July 2011, accepted 29 August 2011
Published online 27 September 2011

Keywords carbon nanotubes, magnetoconductance, Aharonov–Bohm effect, spin–orbit interaction

[*] Corresponding author: e-mail sungho.jhang@physik.uni-regensburg.de, Phone: +49-941-943-1620, Fax: +49-941-943-3196

Magnetoconductance of carbon nanotubes (CNTs) is investigated. We clearly show that a semiconducting CNT can be converted into a metallic one, or vice versa, with the application of a large magnetic field parallel to the tube axis, providing a consistent confirmation of the Aharonov–Bohm (AB) effect on the band structure of CNTs. We also demonstrate that magnetic-field values where the semiconductor-to-metal transition occurs can be tuned by mechanical strain. Combined control of both the strain and the AB effect may open up new possibilities for CNT devices. In addition, we propose an idea to manipulate spin-split subbands of CNTs, resulting from spin–orbit interaction (SOI), by using the magnetic field to generate sizeable spin-polarized currents.

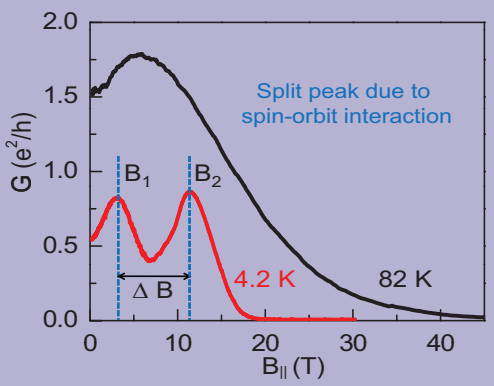

Split magnetoconductance peak due to SOI.

1 Introduction A magnetic field $B_{||}$ parallel to the tube axis provides an efficient tool to manipulate electronic properties of carbon nanotubes (CNTs). The Aharonov–Bohm (AB) phase, picked up by electrons encircling the perimeter of the tube, tunes the periodic boundary condition along the tube circumference and results in a ϕ_0-periodic modulation of band gap [1–3], where $\phi_0 = h/e$ is the flux quantum. Recent experiments demonstrate that one can convert a metallic CNT into a semiconducting one, or vice versa, by engineering the band gap of the tube with $B_{||}$ [4–6]. These magnetically induced changes in the band structure are manifested as large changes in conductance under the magnetic field. On the other hand, perturbations such as mechanical strain [7, 8] and spin–orbit interaction (SOI) [9], which also affect the band structure of CNTs, can be investigated by the conductance measurements in the presence of $B_{||}$ [5, 6]. While the magnetoconductance (MC) of CNTs is often strongly affected by disorder and other quantum interference effects such as Altshuler-Aronov-Spivak oscillations [10], here we deal with the MC in clean CNTs, probed in parallel magnetic fields of up to 60 T.

2 Experiment The experiments have been performed on devices made of individual CNTs, directly grown on $Si/SiO_2/Si_3N_4$ substrates. The heavily p-doped Si was used as a back gate and the thickness of the insulating layer was 350 nm. The CNTs were grown by means of a chemical vapour deposition method [11] and Pd (50 nm) electrodes were defined on top of the tubes by e-beam lithography. The dc two-probe MC was studied in pulsed magnetic fields of up

to 60 T, applied parallel to the tube axis. The accuracy of the alignment was $\sim\pm5^\circ$. The magnetic-field pulse was generated from the discharge of a large capacitor bank and lasted typically $\backsimeq 500$ ms.

3 Magnetoconductance of CNTs

3.1 ϕ_0-periodic modulation of band gap When a magnetic flux ϕ threads through a CNT, the energy gap of metallic CNTs grows linearly with ϕ for $\phi \leq \phi_0/2$, then shrinks back to zero for $\phi_0/2 \leq \phi \leq \phi_0$ (Fig. 1(a)) because of the AB effect [2–5]. For semiconducting CNTs, the initial energy gap closes at $\phi = \phi_0/3$ and then again at $\phi = 2\phi_0/3$ due to two distinct K and K' Dirac points, before recovering its original value at $\phi = \phi_0$ [1, 6]. Figure 1(b) shows an example of the MC for a metallic single-walled CNT, measured at charge neutrality point (CNP) at $V_g = 4.2$ V. The conductance G of the tube exponentially drops several orders of magnitude at $T = 4.2$ K as the energy gap of the tube opens linearly with $B_{||}$. Since actual magnetic fields B_0 equivalent to ϕ_0 are about 5000 and 50 T for CNTs with diameters d of 1 and 10 nm, respectively, here we probe only a few percent of ϕ_0 in the MC of the single-walled CNT ($d \sim 1.5$ nm).

3.2 Aharonov–Bohm beating effect Figure 1(c) displays the MC of the metallic CNT at 4.2 K for various values of gate voltages. The AB effect on the band structure is pronounced only in the vicinity of the CNP. Turning our attention to the MC away from the CNP, the MC trace at $V_g = -6.1$ V shows conductance oscillations with a period of $B_0' \sim 8$ T, much shorter than ϕ_0 (or $B_0 \sim 2000$ T). The G modulations with $B_0' \ll B_0$ can be explained by AB beating effect between two nondegenerate modes of spiraling electrons which encircle the circumference multiple times while traversing the tube length L. The beating modulation period is approximated in Ref. [12] as

$$B_0'(\varepsilon) \approx \frac{\pi d}{L}\frac{\varepsilon}{\varepsilon_g^0}B_0, \tag{1}$$

where ε is the energy and ε_g^0 is the curvature-induced band gap [13] of the metallic CNTs. The G modulations with $B_0' \ll B_0$ result from $d/L \approx 3 \times 10^{-3}$ for our device.

3.3 Semiconductor-to-metal transition and the effect of mechanical strain Figure 2(a) shows the MC trace of an initially semiconducting multi-walled CNT ($d \sim 8$ nm), measured at CNP ($V_g = 4$ V). With the application of $B_{||}$, $G(B_{||})$ exponentially increases by several orders of magnitude to recover the order of one conductance quantum (e^2/h) until it reaches a peak at $B_1 = 22$ T. The conductance then drops back to a minimum around $B_{min} = 37$ T, before increasing towards the second peak. The large consecutive change in G agrees in general with the band-gap modulation due to the AB effect (Fig. 1(a)). The conductance peak at $B_1 = 22$ T and the minimum at $B_{min} = 37$ T can be attributed to the band-gap closure at $\phi = \phi_0/3$ and a local E_g maximum at $\phi = \phi_0/2$, respectively. However, $d = 8 \pm 0.5$ nm, determined from atomic force microscope, rather suggests $24.5\,\text{T} \leq \phi_0/3 \leq 31.5\,\text{T}$ [see the bar in Fig. 2(a)]. Also, if $B_1 = 22$ T corresponds to the band-gap closure at $\phi = \phi_0/3$, then the second peak should already appear at $B_2 = 44$ T. Recently, we have shown that the shifted positions of the MC peaks can be explained by the effect of mechanical strain in CNTs [6]. In the presence of an axial strain, the semiconductor-to-metal transition occurs earlier ($p = -1$) or later ($p = +1$) than at $\phi = \phi_0/3$ depending on the type p of the semiconducting CNT, as shown in Fig. 2(b). Here, $p = \pm 1$ such that the chiral indices (n, m) satisfy $n - m = 3q + p$, with q being an integer. The shift of the MC peak is sensitive to the axial strain especially for larger diameter tubes (Fig. 3(a)), and a small axial strain of $\sigma \approx 0.2\%$ can explain the shift of the MC peaks observed in our data, supposing the type of our tube as $p = -1$. The small strain is likely to be present in the device, as this tube was slightly bent during the growth on the SiO_2 substrates. Also, different thermal-expansion coefficients between Si and CNT can play a role, as our tube is fixed to electrodes on the substrate.

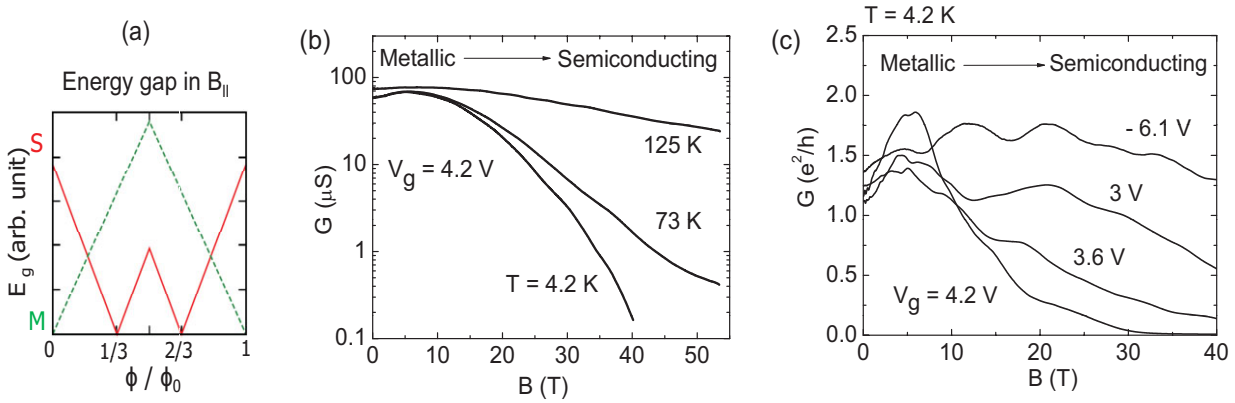

Figure 1 (online colour at: www.pss-b.com) (a) Energy gap in a parallel magnetic field. Solid lines are for initially semiconducting CNTs and dashed lines are for metallic CNTs. (b) MC of a metallic CNT at CNP, measured at three different temperatures. (c) MC traces for various gate voltages at 4.2 K. The CNP is located at $V_g = 4.2$ V.

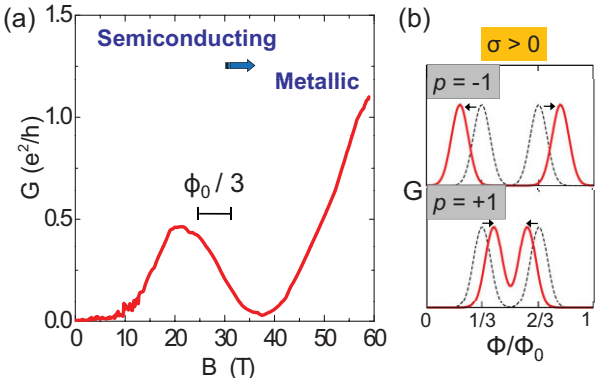

Figure 2 (online colour at: www.pss-b.com) (a) MC of a semiconducting CNT device near the CNP, measured at 3.1 K. (b) Shift of MC peaks under strain $\sigma > 0$. Solid and dashed lines are with and without the strain, respectively. The two peaks at $\phi = \phi_0/3$ and at $\phi = 2\phi_0/3$ move either closer (for $p = +1$) or away from each other (for $p = -1$).

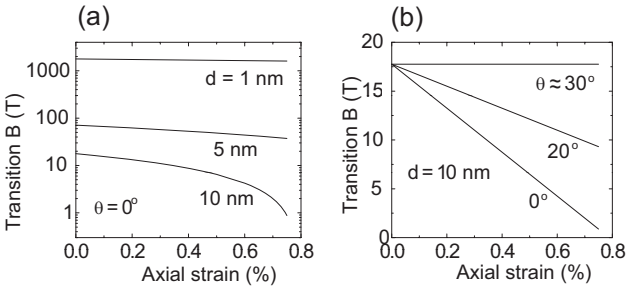

Figure 3 (a) Magnetic fields where semiconductor-to-metal transitions occur for zigzag tubes with $p = -1$ under axial strain. (b) Field values where the transition occurs for a 10 nm diameter tube under axial strain and its chiral angle dependence.

While previous researchers have been mostly focusing on either the parallel magnetic field or the axial strain to tune the band structure of CNTs, our findings suggest that the combined control of both may open up new possibilities for magneto-electronic and magneto-optical CNT devices. For example, the semiconductor-to-metal transition would occur at 17 T (actual field equivalent to $\phi_0/3$) for a 10 nm diameter tube, but we can make, in principle, the transition occur at any smaller value by controlling the axial strain in the tube, except nearly armchair CNTs (Fig. 3(b)).

3.3.1 Effect of torsional strain Not only the axial strain σ but also torsional strain γ can affect the MC of the CNTs in a similar manner. The shift of the K-points, which leads to the shifted positions of MC peaks, depends on σ, γ, and the chiral angle θ, and is given by Ref. [7]

$$\Delta k_\perp = \tau a_0^{-1}[(1+\nu)\sigma\cos(3\theta) + \gamma\sin(3\theta)],$$
$$\Delta k_\parallel = \tau a_0^{-1}[-(1+\nu)\sigma\sin(3\theta) + \gamma\cos(3\theta)], \quad (2)$$

where $\tau = \pm 1$ for the K and K' Dirac points, a_0 is the C–C bond length, and ν is the Poisson ratio. As a result, the two MC peaks at $\phi = \phi_0/3$ and at $\phi = 2\phi_0/3$ move either closer (for $p = +1$) or away from each other (for $p = -1$) under both torsional and axial strain, but with different chiral angle dependence. While the effect of axial strain is largest for zigzag CNTs ($\theta = 0^\circ$), the effect of torsional strain is largest for armchair CNTs ($\theta = 30^\circ$).

3.4 Spin-polarization by SOI Whereas in flat graphene the SOI is very weak, the geometric curvature in CNTs enhances the effective strength of the SOI by several orders of magnitude. A recent experiment has demonstrated the effect of SOI in clean CNT quantum dots [9]. As shown in Fig. 4(a), the spin-orbit coupling splits the commonly assumed fourfold degeneracy (2 spin × 2 orbital) into two pairs of spin and orbital orientations; an effective flux ϕ_{SO} corresponding to the spin–orbit splitting was estimated to be $\phi_{SO} \approx 10^{-3}\phi_0$ in agreement with theoretical predictions [14, 15]. Considering that the actual $B_{||}$ equivalent to ϕ_0 is about 5000 T for a CNT with $d \sim 1$ nm, the effect of the spin-orbit splitting should then appear in the MC on a scale of a few T for single-walled CNT devices. Indeed, we observed a peculiar splitting of the MC peak ($\Delta B = 8$ T) for a chiral metallic CNT (see the abstract figure), which can be explained in terms of spin-split conduction bands, separated by the SOI [5]. With increasing $B_{||}$, the spin-split sub-bands shift due to the AB effect and cross the K-point, successively closing the energy gap at B_1 and B_2. As illustrated in Fig. 4(b), the current in the MC peaks at B_1 and B_2 can be highly spin polarized (in principle up to 100%). The measured MC is of the order of the conductance quantum, which in our experiment corresponds to sizeable polarized currents, up to a micro-Ampere. Thus, we demonstrate the possibility of using CNTs as highly efficient ballistic spin filters.

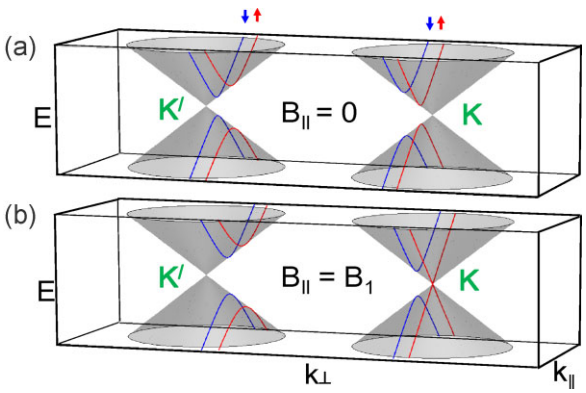

Figure 4 (online colour at: www.pss-b.com) Spin-polarization by SOI. (a) Dirac cones near the K-points, intersected by lines of allowed $k_\perp$ values for a small-bandgap CNT with SOI. 1D dispersion curves are determined by the cut of Dirac cones with vertical planes of allowed $k_\perp$. Spin-up and spin-down bands (marked by arrows) are separated due to the SOI. (b) With increasing $B_{||}$, spin-split sub-bands shift due to the AB effect and cross the K point at $B_{||} = B_1$, possibly leading to a complete spin polarization of transmitted channels in CNTs.

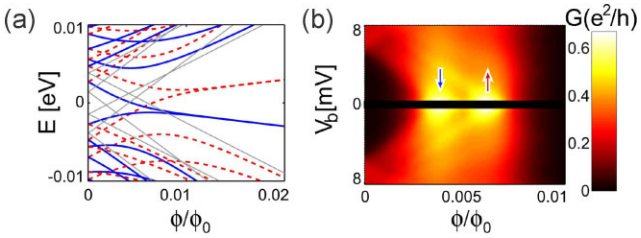

Figure 5 (online colour at: www.pss-b.com) (a) Spin-resolved energy spectrum for a (12,9) CNT with a length of 518 nm. The dashed lines in the analytical calculation correspond to spin-up states and the solid lines to spin down. The parameters for the calculations are given in Ref. [19]. The superimposed gray lines indicate the edge of the bands in the case of an infinite CNT. (b) Integrated conductance for the same CNT. The points around $V_b = 0$ have been suppressed in order to avoid a division by zero.

3.4.1 Interplay between the SOI and Zeeman effect The Zeeman effect splits antiparallel spin states and reduces the band gap by $\Delta E_Z \approx 0.1\ \mathrm{meV/T} \cdot B_{||}$, affecting the ϕ_0-periodic modulation of the band gap [16]. On the other hand, spin-orbit splitting in energy is inversely proportional to the diameter, and given by $\Delta_{SO} \approx 1.9/d$ meV nm. For semiconducting CNTs, the MC peak at $\phi = \phi_0/3$ does not split into two, as the Zeeman contribution at $\phi = \phi_0/3$ ($\Delta E_Z \approx 200/d^2$ meV nm^2) is much larger than the Δ_{SO}. For the tube with d of 8 nm, $\Delta E_Z \approx 3$ meV and $\Delta_{SO} \approx 0.2$ meV at $\phi = \phi_0/3$. For the same reason, the split MC peak is found in metallic tubes close to the armchair configuration [5], where the curvature-induced band gap is small.

3.4.2 Effect of finite size of the CNT It is theoretically shown that in finite zigzag and chiral CNTs extended states become localized in an applied parallel magnetic field [17, 18]. This localization occurs at the ends of the CNT and causes a gradual suppression of the conductance. Since this phenomenon takes place in the vicinity of the Fermi energy, it is relevant in transport properties at low energies.

Figure 5 presents conductance calculations performed for a chiral metallic CNT with a length similar to our measured device. The SOI and Zeeman effect cause a separation of the spin species and an electron–hole asymmetry, and localized states cross the Fermi energy at different magnetic fields for spin up and down. The MC shows the double-peak feature as experimentally observed in our CNT, and each peak corresponds to a highly polarized current [19]. The separation in magnetic flux of these peaks is determined by several factors, such as tube chirality, diameter and length. A longer CNT will show a larger separation of the MC peaks.

4 Summary We have investigated the MC of CNTs up to very high magnetic fields. In addition to the confirmation of the AB effect on the band structure of CNTs, we show the important influence of mechanical strain on the MC of the CNTs. We also demonstrate the possibility of using CNTs as ballistic spin filters by exploiting the SOI.

Acknowledgements We acknowledge B. Witkamp and H. van der Zant for help in the growth of CNTs. This research was supported by the Deutsche Forschungsgemeinschaft within GRK 1570 and SFB 689 and by EuroMagNET under the EU Contract No. 228043.

References

[1] H. Ajiki and T. Ando, J. Phys. Soc. Jpn. **62**, 1255 (1993). J. P. Lu, Phys. Rev. Lett. **74**, 1123 (1995). S. Roche, G. Dresselhaus, M. S. Dresselhaus, and R. Saito, Phys. Rev. B **62**, 16092 (2000).
[2] U. C. Coskun, T.-C. Wei, S. Vishveshwara, P. M. Goldbart, and A. Bezryadin, Science **304**, 1132 (2004).
[3] B. Lassagne, J.-P. Cleuziou, S. Nanot, W. Escoffier, R. Avriller, S. Roche, L. Forró, B. Raquet, and J.-M. Broto, Phys. Rev. Lett. **98**, 176802 (2007).
[4] G. Fedorov, A. Tselev, D. Jiménez, S. Latil, N. G. Kalugin, P. Barbara, D. Smirnov, and S. Roche, Nano Lett. **7**, 960 (2007). G. Fedorov, P. Barbara, D. Smirnov, D. Jiménez, and S. Roche, Appl. Phys. Lett. **96**, 132101 (2010).
[5] S. H. Jhang, M. Margańska, Y. Skourski, D. Preusche, B. Witkamp, M. Grifoni, H. van der Zant, J. Wosnitza, and C. Strunk, Phys. Rev. B **82**, 041404(R) (2010).
[6] S. H. Jhang, M. Margańska, Y. Skourski, D. Preusche, M. Grifoni, J. Wosnitza, and C. Strunk, Phys. Rev. Lett. **106**, 096802 (2011).
[7] L. Yang and J. Han, Phys. Rev. Lett. **85**, 154 (2000).
[8] E. D. Minot, Y. Yaish, V. Sazonova, J.-Y. Park, M. Brink, and P. L. McEuen, Phys. Rev. Lett. **90**, 156401 (2003).
[9] F. Kuemmeth, S. llani, D. C. Ralph, and P. L. McEuen, Nature (London) **452**, 448 (2008).
[10] A. Bachtold, C. Strunk, J.-P. Salvetat, J.-M. Bonard, L. Forró, T. Nussbaumer, and C. Schönenberger, Nature (London) **397**, 673 (1999). G. Fedorov, B. Lassagne, M. Sagnes, B. Raquet, J.-M. Broto, F. Triozon, S. Roche, and E. Flahaut, Phys. Rev. Lett. **94**, 066801 (2005). B. Stojetz, C. Miko, L. Forró, and C. Strunk, Phys. Rev. Lett. **94**, 186802 (2005).
[11] J. Kong, H. T. Soh, A. M. Cassell, C. F. Quate, and H. Dai, Nature (London) **395**, 878 (1998).
[12] J. Cao, Q. Wang, M. Rolandi, and H. Dai, Phys. Rev. Lett. **93**, 216803 (2004).
[13] C. L. Kane and E. J. Mele, Phys. Rev. Lett. **78**, 1932 (1997).
[14] T. Ando, J. Phys. Soc. Jpn. **69**, 1757 (2000).
[15] D. Huertas-Hernando, F. Guinea, and A. Brataas, Phys. Rev. B **74**, 155426 (2006).
[16] J. Jiang, J. Dong, and D. Y. Xing, Phys. Rev. B **62**, 13209 (2000).
[17] K. Sasaki, S. Murakami, R. Saito, and Y. Kawazoe, Phys. Rev. B **71**, 195401 (2005).
[18] M. Margańska, M. del Valle, S. H. Jhang, C. Strunk, and M. Grifoni, Phys. Rev. B **83**, 193407 (2011).
[19] M. del Valle, M. Margańska, and M. Grifoni, Phys. Rev. B (in press), arXiv: 1103 2308v1.